ELSEVIER

www.elsevier.nl/locate/jorganchem

Journal of Organometallic Chemistry 608 (2000) 42–48

Journal of Organometallic Chemistry

Bonding studies of dinuclear transition metal bis(μ-η^2-silane) complexes $[L_nM(\mu\text{-}\eta^2\text{-}HSiR_2)]_2$ by density functional theory

Sai-Heung Choi, Zhenyang Lin *

Department of Chemistry, Hong Kong University of Science and Technology, Clear Water Bay, Kowloon, Hong Kong

Received 21 May 2000; received in revised form 26 May 2000

Abstract

The bonding and structural features of a series of dinuclear transition metal bis(μ-η^2-silane) complexes $[L_nM(\mu\text{-}\eta^2\text{-}HSiR_2)]_2$ were studied using density functional theory calculations. These dinuclear complexes consist of two metal fragments doubly bridged by two (μ-η^2-HSi) units with a formal metal–metal bond. Each metal fragment conforms to either the 16- or 18-electron rule dependent on the spatial arrangement of ligands around each metal coordination sphere. These dinuclear silane complexes display noticeably shorter Si···H distances in the $[M(\mu\text{-}\eta^2\text{-}HSi)]_2$ units when compared with mononuclear η^2-silane complexes. The shorter Si···H distances in the metal–(η^2-silane) interactions suggest that these dinuclear complexes are more non-classical than mononuclear ones. The more non-classical feature is a result of weaker metal(d) to Si–H(σ*) back-donation interactions due to the presence of a metal substituent at silicon. © 2000 Elsevier Science S.A. All rights reserved.

Keywords: Bonding analyses; Density functional calculations; Dinuclear metal–silane complexes

1. Introduction

Studies of transition metal η^2-silane complexes have been one of the active research areas in the past two decades [1,2]. The majority of transition metal η^2-silane complexes characterized to date are mononuclear species $[L_nM(\eta^2\text{-}HSiR_3)]$ [3]. A variety of these mononuclear η^2-silane complexes [4–9] including mononuclear bis(η^2-silane) complexes [10,11] have already been well investigated theoretically. In contrast to mononuclear transition metal η^2-silane complexes, dinuclear transition metal η^2-silane complexes $[L_nM(\mu\text{-}\eta^2\text{-}HSiR_2)]_2$, which are summarized in Table 1, are much less common. These complexes are also believed to be involved in catalytic dehydrogenative polymerization [1,12], and dehydrocoupling of secondary silane [13].

Structurally, these dinuclear η^2-silane complexes have an unsymmetrical and planar $[M(\mu\text{-}\eta^2\text{-}HSi)]_2$ core with different M–Si distances. A recently synthesized complex $[(^iPr_2PCH_2CH_2P^iPr_2)(H)Rh(\mu\text{-}\eta^2\text{-}HSiMe_2)]_2$ shows a different structural feature in which the two $[Rh(\mu\text{-}\eta^2\text{-}HSi)]$ units are almost orthogonal to each other [13]. The planar structural feature in most systems and the geometry of this particular rhodium complex are of interest to us. The structural feature of these dinuclear transition metal bis(μ-η^2-silane) complexes has been mentioned briefly [12–21]. However, their bonding characteristics have not yet been systematically studied. In our continuing effort to understand the nature of metal–(η^2-silane) interactions, in this work we attempt to study the bonding feature of these dinuclear transition metal bis(μ-η^2-silane) complexes with the aid of density functional theory calculations. Qualitative bonding pictures [22] will be provided to describe the orbital interactions in the unsymmetrical $[M(\mu\text{-}\eta^2\text{-}HSi)]_2$ structural units of these complexes. Comparisons with mononuclear transition metal η^2-silane complexes will also be made.

2. Computational details

Full geometry optimizations of model complexes of structural types $[LM(\mu\text{-}\eta^2\text{-}HSiH_2)]_2$ (**1a** for M = Pt and **1b** for M = Pd), $[L_3M(\mu\text{-}\eta^2\text{-}HSiH_2)]_2$ (**2** for M = Fe and **3** for M = Rh) and $[L_4M(\mu\text{-}\eta^2\text{-}HSiH_2)]_2$ (**4** for M = W) were performed at the Becke3LYP (B3LYP) [23] level

* Corresponding author. Fax: +852-2358-1594.

0022-328X/00/$ - see front matter © 2000 Elsevier Science S.A. All rights reserved.
PII: S0022-328X(00)00360-0

Table 1. Examples of characterized dinuclear transition metal bis(μ-η²-silane) complexes [a]

Complex	M-M (Å)	Structure
$[LM(\mu\text{-}\eta^2\text{-}HSiR_2)]_2$ (**1**)		
$[P(C_6H_{11})_3Pt(\mu\text{-}\eta^2\text{-}HSiMe_2)]_2$ [17]	2.708	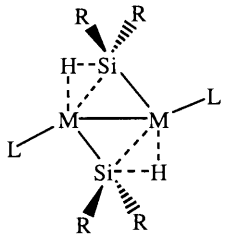
$\{(Pme_2Ph)Pt[\mu\text{-}\eta^2\text{-}HSiH(IMP)]\}_2$ [20]	2.702	
$[(Pme_3)Pd(\mu\text{-}\eta^2\text{-}HSiPh_2)]_2$ [19]	2.691	
$[(PEt_3)Pd(\mu\text{-}\eta^2\text{-}HSiPh_2)]_2$ [21]	2.699	
$[(Pme_3)Pd(\mu\text{-}\eta^2\text{-}HSiMePh)]_2$ [21]	2.707	**1**
$[L_3M(\mu\text{-}\eta^2\text{-}HSiR_2)]_2$		
$[(CO)_3Fe(\mu\text{-}\eta^2\text{-}HSiPh_2)]_2$ [16] (**2**)	2.759	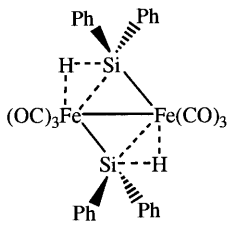
		2
$[(dippe)(H)Rh(\mu\text{-}\eta^2\text{-}HSiMe_2)]_2$ [13] (**3**)	2.858	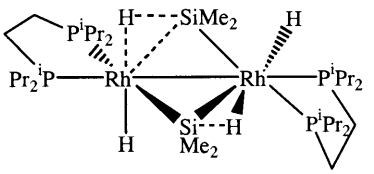
		3
$[L_4M(\mu\text{-}\eta^2\text{-}HSiR_2)]_2$		
$[(CO)_3(P^iPr_3)W(\mu\text{-}\eta^2\text{-}HSiPh_2)]_2$ [18] (**4**)	3.226	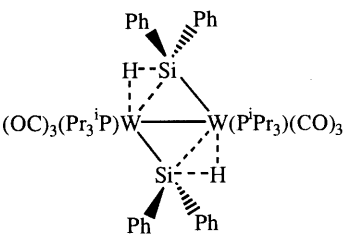
$\{(CO)_4W[\mu\text{-}\eta^2\text{-}HSi(C_2H_5)_2]\}_2$ [14]	3.183	
		4
$[Cp_2M(\mu\text{-}\eta^2\text{-}HSiR_2)]_2$		
$[Cp_2Ti(\mu\text{-}\eta^2\text{-}HSiHPh)]_2$ [12] (**5**)	3.866	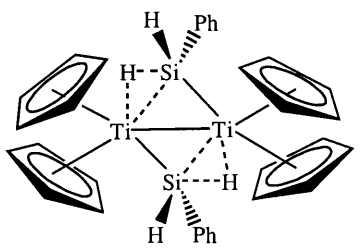
		5

[a] Abbreviation used: ^{i}Pr = isopropyl, Ph = phenyl, dippe = 1,2-bis(diisopropylphosphino)ethane, IMP = 2-isopropyl-6-methylphenyl, Me = methyl.

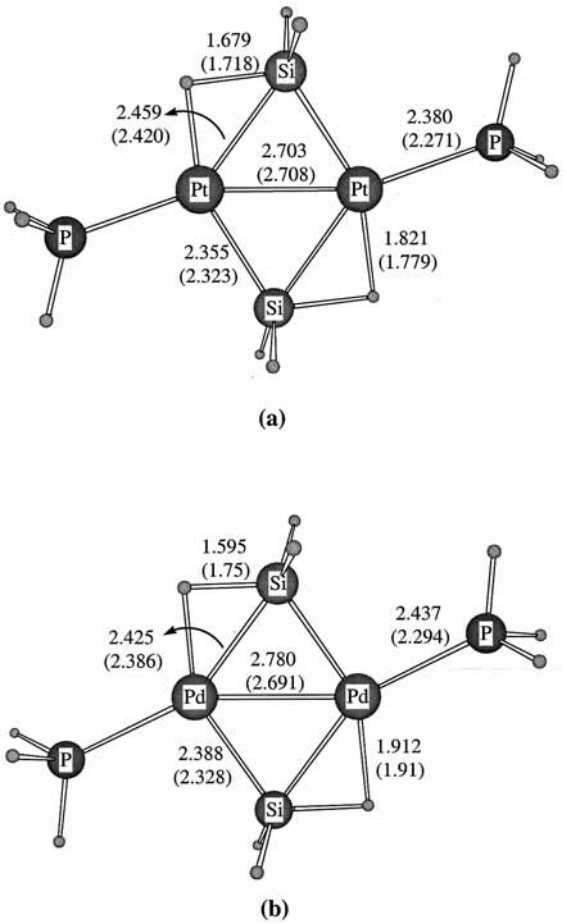

Fig. 1. The B3LYP-optimized and experimentally observed bond lengths (in parenthesis). (a) Model complex $[(PH_3)Pt(\mu\text{-}\eta^2\text{-}HSiH_2)]_2$ (**1a**) and the X-ray determined complex $[P(C_6H_{11})_3Pt(\mu\text{-}\eta^2\text{-}HSiMe_2)]_2$. (b) Model complex $[(PH_3)Pd(\mu\text{-}\eta^2\text{-}HSiH_2)]_2$ (**1b**) and the X-ray determined complex $[(PMe_3)Pd(\mu\text{-}\eta^2\text{-}HSiPh_2)]_2$.

of density functional theory. Here, L represents a neutral two-electron donor ligand (PH_3 or CO). In these model complexes, hydrogen atoms were used to replace alkyl groups in the observed complexes in order to simplify calculations. The effective core potentials (ECPs) of Hay and Wadt with double-ξ valence basis set (LanL2DZ) [24] were used to describe transition metals and atoms in the third period, while the standard 6-31G basis set [25] was used for other atoms. The hydrogen and silicon atoms of the η^2-silane ligands were augmented with polarization functions, namely, p-polarization functions (i.e. 6-31G**) for hydrogen and d-polarization functions of Huzinaga ($\xi = 0.282$) [26] for silicon. All the calculations were performed with the GAUSSIAN98 software package [27] on Silicon Graphics Indigo^2 workstations and PC Pentium III computers. Natural bond order (NBO) analyses were performed using the NBO program [28] as implemented in the GAUSSIAN98 package and the Laplacian ($-\nabla^2\rho$) analysis of electron density was carried out with the MOPLOT package [29].

3. Results and discussion

3.1. $[LM(\mu\text{-}\eta^2\text{-}HSiR_2)]_2$ complexes (M = Pt or Pd)

Complexes belonging to this class have received particular attention among dinuclear transition metal bis(μ-η^2-silane) complexes (see Table 1) [17,19–21]. Model complexes **1a** and **1b**, $[(PH_3)M(\mu\text{-}\eta^2\text{-}HSiH_2)]_2$ with M = Pt and Pd, respectively, were optimized at the B3LYP level of theory. The calculated structural parameters of **1a** and **1b** agree quite well with those of their corresponding observed complexes (Fig. 1). The major discrepancies are only found in the M–P bond distances. At the suggestion of one reviewer, the inclusion of d-polarization functions ($\xi = 0.340$) for phosphorous indeed produces much better results, giving the calculated Pt–P distance (2.289 Å) for **1a** that is very close to the experimental distance (2.271 Å). The use of d-polarization functions of phosphorous does not result in significant changes in the structural parameters related to the $[Pt(\mu\text{-}\eta^2\text{-}HSi)]_2$ core. The Si···H distance in the η^2-silane ligand changes only 0.001 Å. The greatest change (0.04 Å) is found for the Pt–Pt distance (2.744 Å).

The optimized structures of **1a** and **1b** can be described as two distorted square planar metal centers bridged by two η^2-silane ligands as represented by **6**.

Table 2
Calculated Si···H distances (Å) of various mononuclear and dinuclear transition metal η^2-silane complexes, and their corresponding calculation levels [a]

Computationally studied complex	Si···H (Å)	Calculation level
Mononuclear		
$Cp_2Ti(\eta^2\text{-}trans\text{-}HC{\equiv}CSiHMe_2)$ [9]	1.711	MP2
$OsCl(CO)(H)(PH_3)_2(\eta^2\text{-}HSiH_3)$ [5]	1.737	MP2
$cis\text{-}Mo(CO)(PH_3)_4(\eta^2\text{-}HSiH_3)$ [9]	1.813	MP2
$(N_6C_3H_9)Ru(H)(PH_3)(\eta^2\text{-}HSiH_3)$ [7]	1.823	B3LYP
$Ru(H)_2(PH_3)_2[(\eta^2\text{-}HSiH_3)_2(OSiH_2\ \ O)]$ [10]	1.826	B3LYP
$Ru(H)_2(PH_3)_2$	1.842	B3LYP
(κ-η^2-H···SiH_2-*o*-C_2H_2–SiH_2···H) [11]		
$Ru(H)_2(PH_3)_2[(\eta^2\text{-}HSiH_3)_2C_6H_4]$ [10]	1.848	B3LYP
$CpMn(CO)_2(\eta^2\text{-}HSiH_2Me)$ [6]	1.900	MP2
Dinuclear		
$[(PH_3)Pt(\mu\text{-}\eta^2\text{-}HSiH_2)]_2$ (**1a**)	1.679	B3LYP
$[(PH_3)Pd(\mu\text{-}\eta^2\text{-}HSiH_2)]_2$ (**1b**)	1.595	B3LYP
$[(CO)_3Fe(\mu\text{-}\eta^2\text{-}HSiPh_2)]_2$ (**2**)	1.659	B3LYP
$[(PH_3)_2(H)Rh(\mu\text{-}\eta^2\text{-}HSiH_2)]_2$ (**3**)	1.605	B3LYP
$[(PH_3)_2(H)Rh(\mu\text{-}\eta^2\text{-}HSiH_2)]_2$ (**7**)	1.631	B3LYP
$[(CO)_3(PH_3)W(\mu\text{-}\eta^2\text{-}HSiH_2)]_2$ (**4**)	1.617	B3LYP

[a] Abbreviation used: Me = methyl, Tp = hydridotris(pyrazolyl)borate, Cp = η^5-C_5H_5, Cy = cyclohexyl.

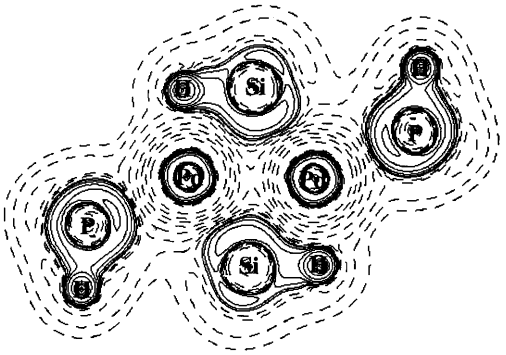

Fig. 2. A Laplacian plot of the electron density of $[(PH_3)Pd(\mu\text{-}\eta^2\text{-}HSiH_2)]_2$ (**1b**) on the plane defined by the $[Pd(\mu\text{-}\eta^2\text{-}HSi)]_2$ unit. Solid lines represent local electron density concentration, and dashed lines represent local density depletion.

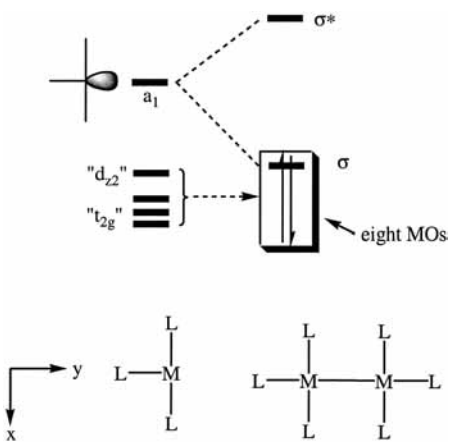

Fig. 3. A schematic orbital interaction diagram for $L_3M\text{–}ML_3$.

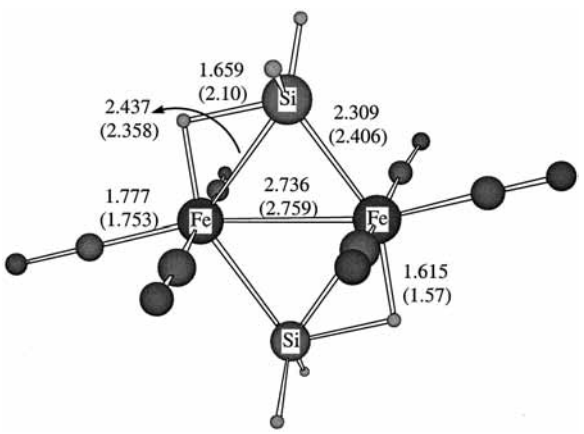

Fig. 4. Selected structural parameters derived from the B3LYP-optimized geometry of $[(CO)_3Fe(\mu\text{-}\eta^2\text{-}HSiH_2)]_2$ (**2**) and the X-ray determined complex $[(CO)_3Fe(\mu\text{-}\eta^2\text{-}HSiPh_2)]_2$ (in parenthesis).

The coordination sphere for each metal center can be viewed as a mononuclear η^2-silane complex with one of the alkyl substituents at Si being replaced by a metal fragment. Thus, it is expected that the structural arrangements around the silicon atom should be more or less the same in both mononuclear and dinuclear η^2-silane complexes.

The non-classical feature of metal–(η^2-silane) interactions **1a** and **1b** can be easily seen, as observed in mononuclear η^2-silane complexes. For example, the bonded M···H distances are significantly longer than the normal terminal metal–hydride distances (< 1.70 Å for both Pt–H and Pd–H) [2,30]. The calculated Si···H distances in the $[M(\mu\text{-}\eta^2\text{-}HSi)]$ units are in the range observed for many other transition metal η^2-silane complexes, but are noticeably shorter than those of mononuclear ones (see Table 2). The shorter Si···H distances suggest that these dinuclear transition metal bis($\mu\text{-}\eta^2$-silane) complexes are more non-classical than their mononuclear analogues. Calculated Si···H distances of some other representative mononuclear η^2-silane complexes are summarized in Table 2. Table 2 clearly shows that the Si···H distances of most calculated mononuclear η^2-silane complexes are within the range of 1.7–1.9 Å, while those of **1a** and **1b** are 1.679 and 1.595 Å, respectively. The shortening of the Si···H distances in these dinuclear transition metal bis($\mu\text{-}\eta^2$-silane) complexes is an indication of decrease in the accepting ability of Si–H(σ*) orbital due to the presence of a metal substituent at Si. The presence of this distal metal as a substituent at Si makes the Si center more electron-rich when compared with the mononuclear ones. The more electron-rich Si center therefore prevents further back-donation interaction of metal(d) to the Si–H(σ*) orbital. The calculated natural charge of Si from the NBO analyses for **1a** and **1b** are 0.46 and 0.41, respectively. These calculated values are indeed less positive than those calculated for the $Cp(CO)_2M(\eta^2\text{-}HSiH_3)$ systems [M = Mn (0.69), Tc (0.67) and Re (0.65)]. In addition to their non-classical features, metal–metal bonding interactions are observed for both **1a** and **1b**, unlike the situation in the dinuclear (μ-silylene) complex, $\{(PMe_2Ph)_2Pt[\mu\text{-}SiH(IMP)]\}_2$ (Pt···Pt distance is 3.962 Å) [20]. The NBO analyses show that the Wiberg bond indices of **1a** and **1b** are 0.15 and 0.11, respectively.

To further elucidate the non-classical feature of these dinuclear transition metal bis($\mu\text{-}\eta^2$-silane) complexes, we analyze the Laplacian of the election density ($-\nabla^2\rho$) [31] of **1b**, on the plane defined by the $[Pd(\mu\text{-}\eta^2\text{-}HSi)]_2$ unit. The Laplacian plot, shown in Fig. 2, shows higher electron density concentrations along the Si···H bond path when compared to other non-classical mononuclear η^2-silane complexes studied previously [9,11]. The Laplacian plots for others show similar features.

In view of the structural and electronic characteristics described above, one can consider these dinuclear complexes as consisting of two T-shaped ML_3 fragments (see **6**), i.e. $L_3M\text{–}ML_3$ if each (η^2-H–Si) moiety is viewed as a pseudo ligand. This simplified consideration significantly benefits the relevant bonding description. A schematic diagram, shown in Fig. 3, illustrates the orbital

interactions between two T-shaped ML_3 fragments. For each T-shaped ML_3 fragment, the frontier fragment orbital a_1 is responsible for the formation of a metal–metal bonding orbital. The 't_{2g}' set and 'd_{z^2}' orbitals give a set of eight approximately non-bonding molecular orbitals. The occupations of these eight orbitals together with the metal–metal bonding orbital lead to a dinuclear complex with an electron count of 30. In other words, the bonding of these dinuclear transition metal bis(μ-η^2-silane) complexes can be described as follows. Each metal center satisfies the 16-electron rule with the presence of a formal metal–metal bond. It is not unexpected that these complexes follow the 16-electron rule since one of the three p orbitals for each metal center is not utilized due to the planar arrangement of ligands around each metal center. The B3LYP calculations clearly show the above-mentioned molecular orbitals for both **1a** and **1b**, giving further support to the orbital interaction argument here.

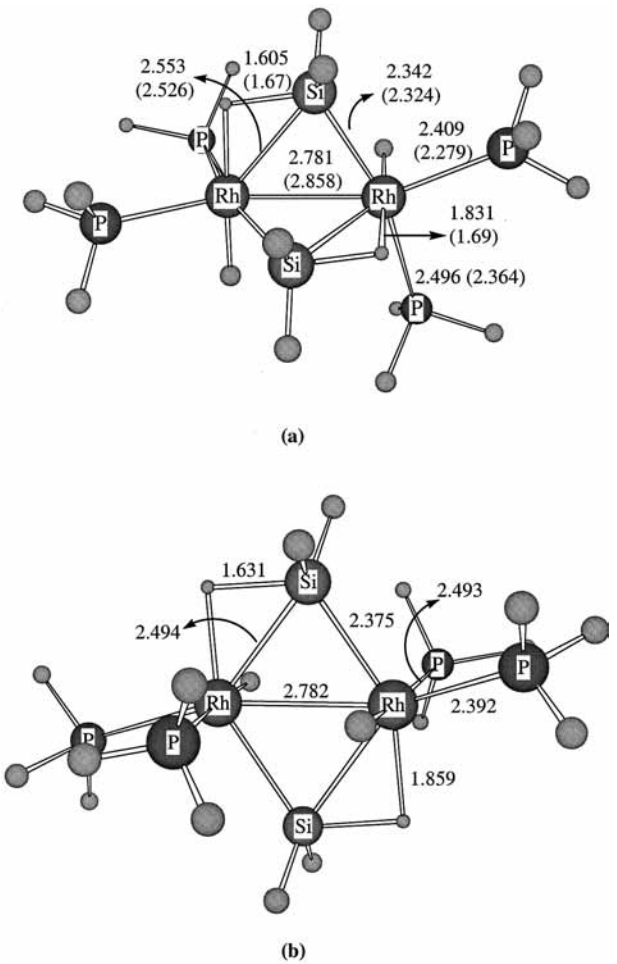

Fig. 5. (a) Selected structural parameters derived from the B3LYP-optimized geometry of $[(PH_3)_2(H)Rh(\mu\text{-}\eta^2\text{-}HSiH_2)]_2$ (**3**) and the X-ray determined complex $[(dippe)(H)Rh(\mu\text{-}\eta^2\text{-}HSiMe_2)]_2$ (in parenthesis). (b) Selected structural parameters of the optimized model complex $[(PH_3)_2(H)Rh(\mu\text{-}\eta^2\text{-}HSiH_2)]_2$ (**7**).

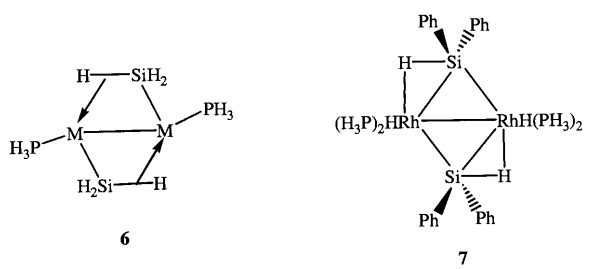

Scheme 1.

3.2. $[L_3M(\mu\text{-}\eta^2\text{-}HSiR_2]_2$ complexes ($M = Fe$ or Rh)

Model complexes $[(CO)_3Fe(\mu\text{-}\eta^2\text{-}HSiH_2)]_2$ (**2**) and $[(PH_3)_2(H)Rh(\mu\text{-}\eta^2\text{-}HSiH_2)]_2$ (**3**) were used to simulate their corresponding observed complexes. The optimized structures of **2** and **3**, respectively illustrated in Figs. 4 and 5(a), are in good agreement with the observed complexes. Major discrepancies are again found in the Rh–P distances. An inclusion of polarization functions for phosphorus should improve the results. Due to the large size of the systems studied here, no further examination was performed. Once again, the Si···H distances in these complexes are shorter than those found in mononuclear η^2-silane complexes (see Table 2). Both optimized structures consist of two metal moieties doubly bridged by two η^2-silane ligands. Each metal center adopts a distorted octahedral geometry if a η^2-silane ligand is considered as a ligand and the metal–metal bond is viewed as a metal–ligand bond. A noticeable structural difference between **2** and **3** is the arrangement of the two bridging η^2-silane ligands. For model **2**, the two bridging η^2-silane ligands are *trans* to each other, allowing the $[Fe(\mu\text{-}\eta^2\text{-}HSi)]_2$ unit of **2** to remain planar (see Fig. 4). The two $[Rh(\mu\text{-}\eta^2\text{-}HSi)]$ units of **3** are almost orthogonal to each other (see Fig. 5(a)).

The non-classical metal–(η^2-silane) interactions in both models **2** and **3** are also clearly indicated by their long M···H and short Si···H distances [2]. Calculated Fe···H and Rh···H distances are 1.615 and 1.831 Å, while the Si···H distances are 1.659 and 1.605 Å, for **2** and **3**, respectively. These results indicate that these dinuclear transition metal bis(μ-η^2-silane) complexes with formula of $[L_3M(\mu\text{-}\eta^2\text{-}HSiR_2]_2$ are again more non-classical than mononuclear η^2-silane complexes. In addition, significant metal–metal interactions are also observed in both complexes. The Wiberg bond indices of **2** and **3** are 0.15 and 0.21, respectively.

It should be noted that the Fe···H distance (1.615 Å) of **2** is only slightly longer than the average Fe–H(terminal) distance (1.575 Å). This suggests that the dinuclear bis(μ-η^2-silane) complex also shows the hydridic character based on the calculated metal–hydrogen distances in spite of the more non-classical nature. In literature, two types of M···H···Si inter-

actions, i.e., M···(H–Si) and M–H···Si, have been discussed. The former type emphasizes the non-classical feature while the latter describes the hydrido–silicon hypervalent interaction [5,11]. The dinuclear bis(μ-η^2-silane) complexes studied here seem to manifest the two types of interactions. Further studies are necessary in order to categorize these bis(μ-η^2-silane) complexes.

Similarly, these complexes can be viewed as a combination of two ML_5 fragments, i.e. $L_5M–ML_5$, despite the different arrangement of the two bridging η^2-silane ligands in **2** and **3**. Each ML_5 fragment has a σ-type hybrid and the 't_{2g}' orbitals. The σ-type hybrid orbital is available for the formation of a metal–metal bond. The 't_{2g}' orbitals remain non-bonding. Full occupations of these non-bonding orbitals together with the metal–metal σ bonding orbital give an electron count of 34. In other words, these complexes conform to the 18-electron rule with a formal metal–metal bond.

To understand the orthogonal arrangement of the two [Rh(μ-η^2-HSi)] units in **3**, model complex **7** with planar $[Rh(\mu\text{-}\eta^2\text{-HSi})]_2$ core was calculated. Selected structural parameters of the optimized structure of **7** are shown in Fig. 5(b) for comparison. It is found that the differences in the relevant bond lengths that involved in the metal–(η^2-silane) interaction between **3** and **7** are small (Fig. 5(a,b)). In addition, computational results show that the energy difference is only 0.17 kcal mol^{-1}, with **7** being more stable. These results suggest that a planar structure is also possible for the Rh complex if adequate ligands are used (Scheme 1).

3.3. $[L_4M(\mu\text{-}\eta^2\text{-HSiR}_2)]_2$ and $[Cp_2M(\mu\text{-}\eta^2\text{-HSiR}_2)]_2$ complexes

Complexes of structural types $[L_4M(\mu\text{-}\eta^2\text{-HSiR}_2)]_2$ **4** and $[Cp_2M(\mu\text{-}\eta^2\text{-HSiR}_2)]_2$ **5** can also be appreciated using similar arguments discussed above. These complexes are isoelectronic to complexes **2** and **3**. Both cases conform to the 18-electron rule with a formal metal–metal bond. The typical structural characteristics, such as the unsymmetrical and planar $[M(\mu\text{-}\eta^2\text{-HSi})]_2$ unit and the non-classical metal–(η^2-silane) interaction, are also found in these dinuclear transition metal bis(μ-η^2-silane) complexes. For the titanium complex $[Cp_2Ti(\mu\text{-}\eta^2\text{-HSiHPh})]_2$ (**5**), the existence of a metal–metal bond may be questionable because of the extremely long Ti···Ti distance (3.866 Å). However, previous computational studies of a similar dimer complex $[Cp_2Zr(\mu\text{-PH}^t\text{Bu})]_2$ also suggest the existence of metal–metal bonding, despite the fact that the metal atoms are separated by more than 3.5 Å [32].

4. Summary

Density functional theory calculations together with molecular orbital interaction arguments have been employed to understand the bonding and structural feature for a variety of dinuclear transition metal bis(μ-η^2-silane) complexes $[L_nM(\mu\text{-}\eta^2\text{-HSiR}_2)]_2$. In general, one can consider these dinuclear complexes as consisting of two metal fragments bridged by two (μ-η^2-HSi) units. A formal metal–metal bond exists between the two metal centers for each complex. In such a consideration, each metal fragment conforms to either the 16- or 18-electron rule depending on the metal coordination sphere in each fragment is planar or not. In these dinuclear transition metal bis(μ-η^2-silane) complexes, our studies indicate that the Si···H distances in the M(μ-η^2-HSi) moieties are noticeably shorter than those found in mononuclear metal η^2-silane complexes. The shorter Si···H distances are explained in terms of weaker metal(d) → Si–H(σ*) back-donation interactions due to the presence of a metal substituents at Si. The metal substituent makes the Si center more electron-rich, and therefore weakens the back-donation interactions. We conclude here that these dinuclear transition metal bis(μ-η^2-silane) complexes are even more non-classical when compared with mononuclear metal η^2-silane complexes. For the $[(dippe)(H)Rh(\mu\text{-}\eta^2\text{-HSiMe}_2)]_2$ complex, our calculation suggests that another structural isomer with a planar $[Rh(\mu\text{-}\eta^2\text{-HSi})]_2$ unit is also possible.

Acknowledgements

This work was supported by the Research Grants Council of Hong Kong and the Hong Kong University of Science and Technology.

References

[1] U. Schubert, Adv. Organomet. Chem. 30 (1990) 151.
[2] J.Y. Corey, J. Braddock-Wilking, Chem. Rev. 99 (1999) 175.
[3] (a) J.K. Hoyano, M. Elder, W.A.G. Graham, J. Am. Chem. Soc. 91 (1969) 4569. (b) W.A.G. Graham, J. Organomet. Chem. 300 (1986) 81. (c) X.-L. Luo, R. H. Crabtree, J. Am. Chem. Soc. 111 (1989) 2527. (d) U. Schubert, Transition Met. Chem. 16 (1991) 136. (e) R.H. Crabtree, Angew. Chem. Int. Ed. Engl. 32 (1993) 789. (f) U. Schubert, M. Schwarz, F. Moller, Organometallics 13 (1994) 1554. (g) X.-L. Luo, G.J. Kubas, J.C. Bryan, C.J. Burns, C.J. Unkefer, J. Am. Chem. Soc. 116 (1994) 10312. (h) A. Ohff, P. Kosse, W. Baumann, A. Tillack, R. Kempe, H. Görls, V.V. Burlakov, U. Rosenthal, J. Am. Chem. Soc. 117 (1995) 10399. (i) J.J. Schneider, Angew. Chem. Int. Ed. Engl. 35 (1996) 1068. (j) F. Delpech, S. Sabo-Etinne, B. Chaudret, J.C. Daran, J. Am. Chem. Soc. 119 (1997) 3167.
[4] H. Rabaâ, J.-Y. Saillard, U. Schubert, J. Organomet. Chem. 330 (1987) 397.
[5] F. Maseras, A. Lledós, Organometallics 15 (1996) 1218.
[6] H. Yang, M.C. Asplund, K.T. Kotz, M.J. Wilkens, H. Frei, C.B. Harris, J. Am. Chem. Soc. 120 (1998) 10154.
[7] S.M. Ng, C.P. Lau, M.-F. Fan, Z. Lin, Organometallics 18 (1999) 2484.

[8] G.I. Nikonov, L.G. Kuzmina, S.F. Vyboishchikov, D.A. Lemenovskii, J.A.K. Howard, Chem. Eur. J. 5 (1999) 2947.
[9] (a) M.-F. Fan, Z. Lin, J. Am. Chem. Soc. 118 (1996) 9915. (b) M.-F. Fan, Z. Lin, Organometallics 16 (1997) 494.
[10] F. Delpech, S. Sabo-Etienne, J. Daran, B. Chaudret, K. Hussein, C.J. Marsden, J. Barthelat, J. Am. Chem. Soc. 121 (1999) 6668.
[11] (a) M.-F. Fan, Z. Lin, Organometallics 17 (1998) 1092. (b) M.-F. Fan, Z. Lin, Organometallics 18 (1999) 286.
[12] (a) C.T. Aitken, J.F. Harrod, E. Samuel, J. Am. Chem. Soc. 108 (1986) 4059. (b) M.D. Fryzuk, L. Rosenberg, S.J. Rettig, Organometallics 10 (1991) 2537.
[13] L. Rosenberg, M.D. Fryzuk, S.J. Rettig, Organometallics 18 (1999) 958.
[14] H. Tobita, H. Ogino, Adv. Organomet. Chem. 42 (1998) 223.
[15] M.J. Bennett, K.A. Simpson, J. Am. Chem. Soc. 93 (1971) 7156.
[16] R.S. Simons, C.A. Tessier, Organometallics 15 (1996) 2604.
[17] M. Auburn, M. Ciriano, J.A.K. Howard, M. Murray, N.J. Pugh, J.L. Spencer, F.G.A. Stone, P. Woodward, J. Chem. Soc. Dalton Trans. (1980) 659.
[18] M.D. Butts, J.C. Bryan, X.-L. Luo, G.J. Kubas, Inorg. Chem. 36 (1997) 3341.
[19] Y.-J. Kim, S.-C. Lee, I. Park, Organometallics 17 (1998) 4929.
[20] Y. Levchinsky, N.P. Rath, J. Braddock-Wilking, Organometallics 18 (1999) 2583.
[21] Y.-J. Kim, S.-C. Lee, J.-I. Park, O. Kohtaro, J.-C. Choi, T. Yamamoto, J. Chem. Soc. Dalton Trans. (2000) 417.
[22] T.A. Albright, J.K. Burdett, M.H. Whangbo, Orbital Interaction in Chemistry, Wiley, New York, 1985.
[23] (a) C. Lee, W. Yang, G. Parr, Phys. Rev. B 37 (1988) 785. (b) B. Miehlich, A. Savin, H. Stoll, H. Preuss, Chem. Phys. Lett. 157 (1989) 200. (c) A. D. Becke, J. Chem. Phys. 98 (1993) 5648.
[24] (a) P.J. Hay, W.R. Wadt, J. Chem. Phys. 82 (1985) 270. (b) W.R. Wadt, P.J. Hay, J. Chem. Phys. 82 (1985) 284. (c) P.J. Hay, W.R. Wadt, J. Chem. Phys. 82 (1985) 299.
[25] P.C. Hariharan, J.A. Pople, Theor. Chim. Acta 28 (1973) 213.
[26] J. Andzelm, S. Huzinaga, Gaussian Basis Sets for Molecular Calculations, Elsevier, New York, 1984.
[27] M.J. Frisch, G.W. Trucks, H.B. Schlegel, G.E. Scuseria, M.A. Robb, J.R. Cheeseman, V.G. Zakrzewski, J.A. Montgomery Jr., R.E. Stratmann, J.C. Burant, S. Dapprich, J.M. Millam, A.D. Daniels, K.N. Kudin, M.C. Strain, O. Farkas, J. Tomasi, V. Barone, M. Cossi, R. Cammi, B. Mennucci, C. Pomelli, C. Adamo, S. Clifford, J. Ochterski, G.A. Petersson, P.Y. Ayala, Q. Cui, K. Morokuma, D.K. Malick, A.D. Rabuck, K. Raghavachari, J.B. Foresman, J. Cioslowski, J.V. Ortiz, B.B. Stefanov, G. Liu, A. Liashenko, P. Piskorz, I. Komaromi, R. Gomperts, R.L. Martin, D.J. Fox, T. Keith, M.A. Al-Laham, C.Y. Peng, A. Nanayakkara, C. Gonzalez, M. Challacombe, P.M.W. Gill, B. Johnson, W. Chen, M.W. Wong, J.L. Andres, C. Gonzalez, M. Head-Gordon, E.S. Replogle, J.A. Pople, GAUSSIAN98 (Revision A.5), Gaussian, Inc, Pittsburgh, PA, 1998.
[28] E.D. Glendening, A.E. Reed, J.E. Carpenter, F. Weinhold, NBO version 3.1.
[29] P. Sherwood, P.J. MacDougall, Interactive MOPLOT: a package for the interactive display and analysis of molecular wave functions, incorporating the programs MOPLOT (D. Lichtenburger), PLOTDEN (R.F.W. Bader, D.J. Kenworthy, P.M. Beddal, G.R. Runtz, S.G. Anderson), SCHUSS (R.F.W. Bader, G.R. Runtz, S.G. Anderson, F.W. Biegler-Koenig), EXTERM (R.F.W. Bader, F.W. Bieger-Koenig), 1989.
[30] R. Bau, M.H. Drabnis, Inorg. Chim. Acta 259 (1997) 27.
[31] R.F.W. Bader, Atoms in Molecules: A Quantum Theory, Clarendon, New York, 1990.
[32] (a) M.M. Rohmer, M. Benard, Organometallics 10 (1991) 157. (b) B. Benard, M.M. Rohmer, J. Am. Chem. Soc. 114 (1992) 4785. (c) R.L. Dekock, M.A. Perterson, L.E.L. Reynolds, L.-H. Chen, E.J. Baerends, P. Vernooijs, Organometallics 12 (1993) 2794. (d) D.W. Stephan, Angew. Chem. Int. Ed. Engl. 39 (2000) 314.